The Journal of Neuroscience, February 1992, 12(2): 525–537

Modulatory Effects of FMRF-NH_2 on Outward Currents and Oscillatory Activity in Heart Interneurons of the Medicinal Leech

Ted W. Simon, Clifford A. Opdyke, and Ronald L. Calabrese

Department of Biology, Emory University, Atlanta, Georgia 30322

Using single-electrode voltage clamp, heart interneurons of the medicinal leech were shown to possess both a rapidly inactivating outward current, I_A, and a more slowly inactivating outward current, I_K. I_A and I_K could be separated by their voltage sensitivity and kinetic properties. FMRF-NH_2 (Phe-Met-Arg-Phe-NH_2) modulates I_K by shifting both steady state activation and inactivation to more hyperpolarized potentials, but it does not affect the time constants.

I_A and I_K appear to use K^+ as a charge carrier; a change in the external [K^+] produced a shift in the apparent reversal potential in the direction predicted with potassium as the charge carrier. Both I_A and I_K are sensitive to tetraethylammonium (TEA) and 4-aminopyridine (4-AP), and TEA and 4-AP both interfere with the effects of FMRF-NH_2 on I_K.

The biophysical properties of I_A and of I_K in the presence and absence of FMRF-NH_2 were incorporated into a Hodgkin–Huxley model of these currents that could reproduce voltage-clamp data.

FMRF-NH_2 produces two apparently dissimilar effects on the heartbeat rhythm—acceleration and disruption. We suggest that both effects could result from the hyperpolarizing shifts in steady state activation and inactivation of I_K.

As a leech begins to swim, the increased metabolic demands of swimming may require a greater cardiac output—an increase in heart rate. Cell 204, a swim-initiating interneuron (Weeks and Kristan, 1978), contains FMRF-NH_2 (Phe-Met-Arg-Phe-NH_2)-like immunoreactivity (Kuhlman et al., 1985a), and its stimulation can increase the centrally generated heart rate (Arbas and Calabrese, 1984). Bath application of FMRF-NH_2 at low concentrations (10^{-8}–10^{-9} M) can accelerate the cycling of the leech heartbeat pattern generator, but higher concentrations ($>10^{-7}$ M) tend to disrupt the rhythm (Kuhlman et al., 1985b).

The leech heartbeat pattern generator is composed of seven bilateral pairs of heart interneurons in the seven anterior segmental ganglia. The interneurons in this pattern generator control heartbeat timing and coordination in the absence of sensory feedback (Thompson and Stent, 1976; Calabrese, 1977). Each of the pairs of heart interneurons in the third and fourth segmental ganglia forms reciprocal inhibitory synapses across the ganglionic midline. Normal electrical activity in heart interneurons consists of depolarized plateaus and bursts of actions potentials (plateau/burst phases) alternating with periods of inhibition (inhibited phase) with a period of 6–15 sec at room temperature (Thompson and Stent, 1976; Calabrese et al., 1989) (see Fig. 13).

One can consider the effect of FMRF-NH_2 on leech heart interneurons to be a modification of neuronal excitability that is of long duration relative to synaptic events. Other long-term changes in neuronal excitability have, in some cases, been shown to be due to modulatory changes in voltage-gated K^+ currents (Kupfermann, 1979; Aghajanian, 1985; Marder and Hooper, 1985; Harris-Warwick and Flamm, 1987; Jones and Adams, 1987; Madison et al., 1987; Siegelbaum, 1987; Strong and Kaczmarek, 1987; Marder and Meyrand, 1989; Marder and Nusbaum, 1989).

In this study, we use single-electrode voltage clamp to determine the kinetic properties of the outward currents I_A and I_K and show that bath-applied FMRF-NH_2 affects I_K. A large fraction of both these currents is dependent on both internal and external Ca^{2+}. Our data show that both currents are blocked by known potassium channel blockers tetraethylammonium (TEA) and 4-aminopyridine (4-AP) and that the magnitude of I_K is dependent on external [K^+]. FMRF-NH_2 shifts both steady state activation and inactivation of I_K to more hyperpolarized potentials but apparently has no effect on the corresponding time constants. We describe a Hodgkin–Huxley model of the outward currents with FMRF-NH_2 modulation acting on I_K. Finally, we demonstrate the effects of bath-applied FMRF-NH_2 on the cycle rate and pattern recorded from oscillatory pairs of heart interneurons.

Materials and Methods

Animals and preparation. Leeches, *Hirudo medicinalis,* were obtained from Leeches USA (NY) and maintained in artificial pond water at 15°C. Animals were anesthetized in ice-cold saline, and individual ganglia were dissected. Ganglia were pinned ventral side up in Sylgard (Dow-Corning)-lined Petri dishes (bath vol, 0.5 ml), and the connective tissue sheath over the neuronal somata was removed with fine scissors. We examined heart interneurons in segmental ganglia 3, 4, 6, and 7 and found no differences in the outward currents in different ganglia.

Solutions, electrodes, and electronics. Ganglia were initially superfused (1.5 ml/min) with normal leech saline containing (in mM) NaCl, 115; KCl, 4; $CaCl_2$, 1.8; glucose, 10; HEPES, 10; pH 7.4. Equimolar amounts of *N*-methyl-D-glucamine and Co^{2+} replaced Na^+ and Ca^{2+}, respectively, in 0 Na^+, 0 Ca^{2+} salines. For determination of Ca^{2+} dependence of the outward currents, the concentration of Ca^{2+} or Co^{2+} in the saline was increased to 5 mM.

FMRF-NH_2 (BaChem) was dissolved in HPLC-grade water (VWR) at a concentration of 5 mg/ml, stored frozen, and dissolved in saline immediately prior to use.

Intracellular recordings were made with borosilicate microelectrodes (1 mm o.d., 0.75 mm i.d.) filled with (1) 4 M K-acetate with 20 mM KCl (25–35 MΩ); (2) 1.8 M tetraethylammonium-acetate (TEA), 2 M

Received Mar. 14, 1991; revised Sept. 17, 1991; accepted Sept. 23, 1991.

We thank Dr. P. Jeffrey Conn, Dr. Isabelle Gourdon-Duchatelle, and Dr. Louis DeFelice for helpful discussions. This work was supported by NIH Grant NS24072 to R.L.C. and NRSA Fellowship NS08394 to T.W.S.

Correspondence should be addressed to Ronald L. Calabrese, Department of Biology, Emory University, 1510 Clifton Road, Atlanta, GA 30322.

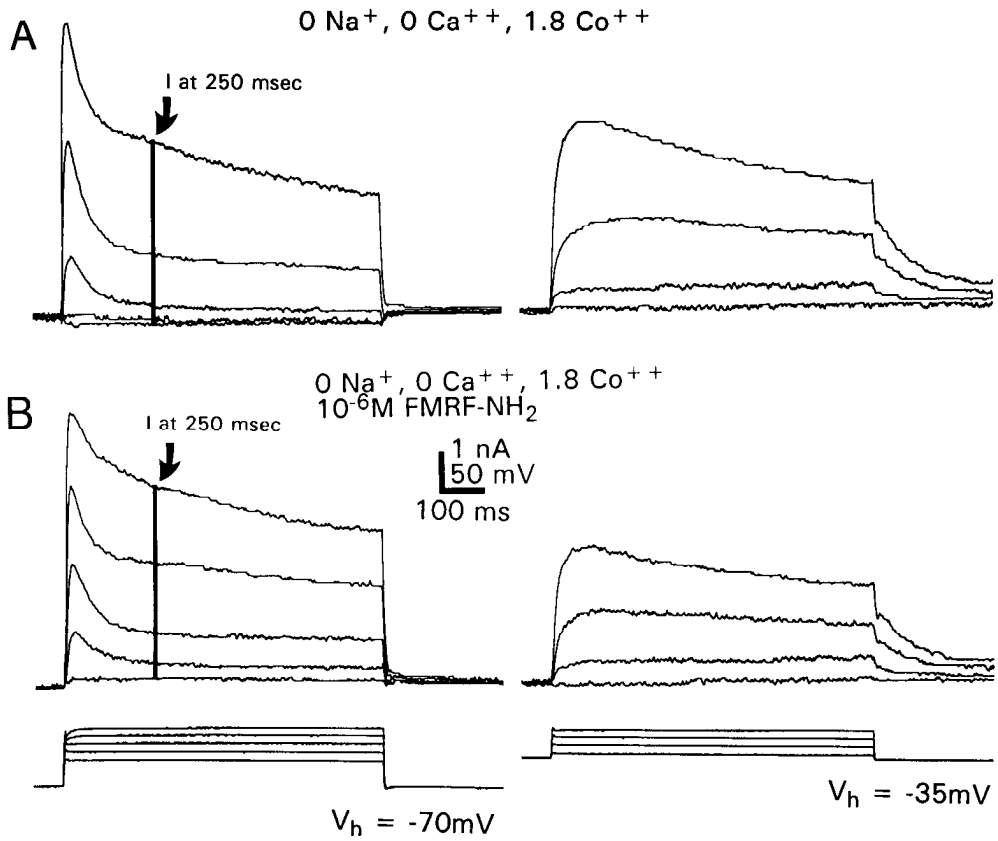

Figure 1. Paradoxical effects of FMRF-NH_2 on I_K. *A*, The *left panel* shows currents evoked by step depolarizations to −40 mV, −30 mV, −20 mV, −10 mV, and 0 mV from a holding potential of −70 mV. The *right panel* shows currents evoked by step depolarizations to −30 mV, −20 mV, −10 mV, and 0 mV from a holding potential of −35 mV. *B*, The *left* and *right panels* show currents evoked by a similar voltage protocol as in *A* in the presence of 10^{-6} M FMRF-NH_2. The line marked *I at 250 msec* in the *left panels* of both *A* and *B* indicates the point at which I_K was measured when elicited from a holding potential of −70 mV. After 250 msec, I_A has inactivated to less than 10% of its peak amplitude, and the current at this time is a measure of I_K.

K-acetate with 10 mM KCl (35–50 MΩ); or (3) 0.2 M bis(2-aminophenoxy)ethane-*N,N,N',N'*-tetraacetate (BAPTA), 2 M K-acetate with 20 mM KCl (25–45 MΩ).

Currents were measured with a switching single-electrode voltage clamp (Axoclamp 2A, Axon Instruments, Foster City, CA). In single-electrode voltage clamp, the voltage input to the sample and hold circuit was monitored to ensure complete electrode settling between current injection cycles. Sample rates ranged between 2.5 and 6 kHz, and clamp gain, from 8 to 25 nA/mV. The output bandwidth was either 0.3 or 1 kHz with higher and lower sample rates, respectively. Voltage-clamp data were digitized and later analyzed using a personal computer with pCLAMP software (Axon Instruments). Voltage recordings were made with the voltage clamp in bridge mode and were acquired on a VHS video recorder modified for FM recording (Vetter Instruments, Chambersburg, PA).

Experimental protocol for voltage clamp. Voltage steps were generated by the voltage clamp and triggered with the computer. Several seconds were allowed to elapse between voltage pulses, ensuring removal of inactivation of the currents under study. Generally, depolarizing steps were followed by hyperpolarizing steps of equal duration and magnitude. The hyperpolarizing steps were used to obtain leak currents for leak subtraction. When complex protocols were used (e.g. see Figs. 5, 11), separate leak steps were performed following the entire series of depolarizing steps.

Modeling. Computer programs for voltage-clamp simulations (MACROCHAN) (DeFelice et al., 1985) and curve fitting (FIT) were supplied by Mr. Bill Goolsby of the Department of Anatomy and Cell Biology of Emory University. Equations describing the dependence of rate constant on membrane potential were obtained by the Marquardt method of iterative least squares. The rate constant equations were the familiar Boltzmann-type equations (Hodgkin & Huxley, 1952b; Beeler and Reuter, 1977; Yamada et al., 1989) (see Results for details).

Results

I_A and I_K are present in leech HN interneurons

We measured leak-subtracted total outward current in 0 Na^+, 0 Ca^{2+}, 1.8 Co^{2+} saline. Two outward currents were present and could be separated on the basis of their voltage sensitivity. At a holding potential of −70 mV, both a rapidly inactivating current similar to I_A (Connor and Stevens, 1971) and a large, slowly inactivating current similar to the delayed rectifier or I_K (Hodgkin and Huxley, 1952a) were observed (Fig. 1*A*, left). At a holding potential of −35 mV, only I_K was observed (Fig. 1*A*, right).

Paradoxical effects of FMRF-NH_2 on the amplitude of I_K

We examined the effect of bath-applied FMRF-NH_2 on outward currents in leech heart interneurons. In the absence of FMRF-NH_2, I_K was initially activated at −20 mV from a holding potential of −70 mV (Fig. 1*A*, left). When the peptide was added, I_K was first activated at −30 mV, and perhaps to a small extent at −40 mV (Fig. 1*B*, left). In addition, the amplitude of I_K was larger at all test potentials in FMRF-NH_2. However, when elicited from a holding potential of −35 mV, I_K was reduced at all test potentials (Fig. 1*B*, right). Thus, FMRF-NH_2 paradoxically increased the amplitude of I_K from a holding potential of −70 mV and reduced it from a holding potential of −35 mV. We observed similar effects of FMRF-NH_2 in over 20 different preparations but were unable to observe a consistent effect of FMRF-NH_2 on I_A.

Kinetic and steady state parameters of I_K

Steady state activation values for I_K were determined by holding the cell at −35 mV and stepping for 800 msec to a range of test depolarizations (Fig. 2*A*). Conductance values were calculated based on a reversal potential of −75 mV (see Fig. 5 and caption). These values were normalized by fitting them to a general steady state equation

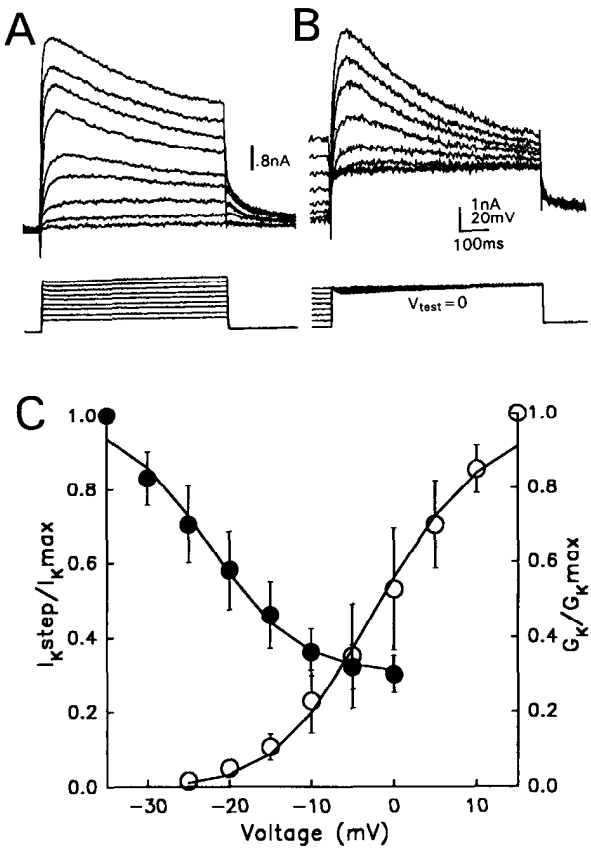

Figure 2. Steady state activation and inactivation of I_K. *A*, Representative currents activated from a holding potential of −35 mV by a series of depolarizing steps from −25 mV to +15 mV. *B*, Currents obtained by stepping to a test potential of 0 mV after inactivation by a series of depolarized holding potentials. In *A* and *B*, voltage traces are shown below the corresponding currents. *C*, Average steady state activation (*open circles*, means ± SEM; $n = 8$) and inactivation (*solid circles*, means ± SEM; $n = 6$) of I_K versus voltage. The *smooth curves* were calculated using Equation 1 with G_{max} assumed to be unity and using the values in Table 1.

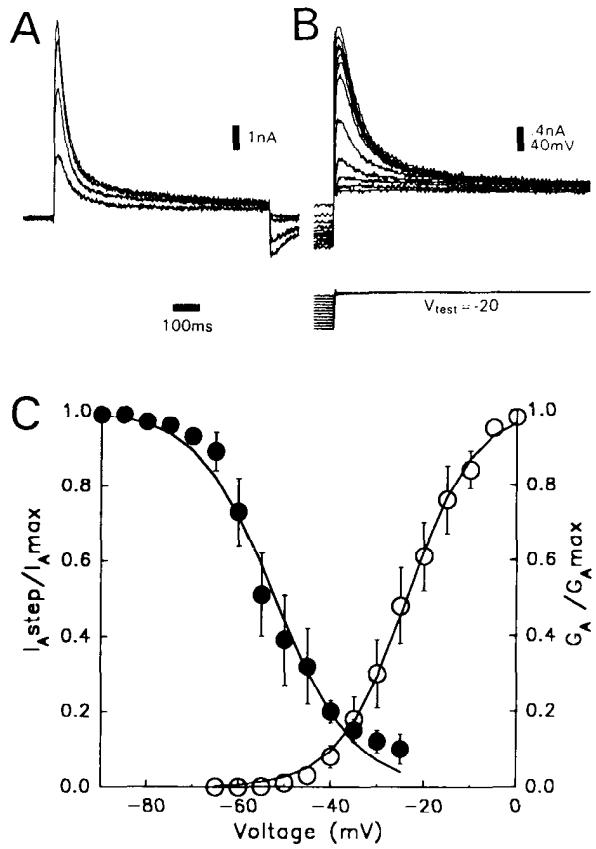

Figure 3. Steady state activation and inactivation of I_A. *A*, Isolation of I_A by subtracting currents elicited by depolarizing steps from a holding potential of −35 mV from currents obtained by steps to like potentials from a holding potential of −70 mV (compare Fig. 1*A*). This subtraction procedure was our usual method for isolating I_A. *B*, Currents obtained by stepping to a test potential of −20 mV after inactivation by a series of depolarized holding potentials. *C*, Average steady state activation (*open circles*, means ± SEM; $n = 6$) and inactivation (*solid circles*, means ± SEM; $n = 5$) of I_A versus voltage. The *smooth curves* were calculated using Equation 1 with G_{max} assumed to be unity and using the values in Table 1.

$$G(V) = \frac{G_{max}}{1 + \exp((V + \text{offset})/\text{slope})} \quad (1)$$

and dividing each value by G_{max}. The numerical values for G_{max}, slope, and offset are shown in Table 1. This normalization procedure converted conductance to steady state activation. Steady state activation values were averaged ($n = 8$) and plotted versus membrane potential (Fig. 2*C*, open circles). The fit of Equation 1 with G_{max} taken as unity is also shown (Fig. 2*C*, line that follows the open circles).

Steady state inactivation values for I_K were determined by maintaining the cell for 2 sec at different holding potentials and then stepping to an activating test potential of 0 mV (Fig. 2*B*). The holding potentials were increased in 5 mV increments from −35 mV to −5 mV in successive trials. Steady state inactivation was calculated as the ratio between the peak current obtained during the test pulse and the peak current from a holding potential of −35 mV. Steady state inactivation values were averaged ($n = 6$) and plotted versus holding potential (Fig. 2*C*, solid circles). I_K was first activated at −20 mV and failed to reach a saturating conductance at +15 mV. I_K did not completely inactivate; 20–40% of the current remained after holding at 0 mV. Steady state inactivation (Fig. 2*C*, line that follows solid circles) of I_K was fit to

$$h_\infty = 0.7\frac{1}{1 + \exp((V + \text{offset})/\text{slope})} + 0.3. \quad (2)$$

I_K inactivated with a single exponential time constant ranging from 735 ± 276 msec at −10 mV ($n = 6$) to 459 ± 67 msec at + 15 mV ($n = 5$) (see Fig. 12). The time constant of removal of inactivation of I_K was 1.46 ± 0.13 sec ($n = 5$).

Table 1. Values used in the conductance equation (Eq. 1) for I_A and I_K

Steady state parameter		G_{max}	Slope	Offset
I_A	m_∞	79.6	−7.62	−8.27
	h_∞		−22.53	5.43
I_K	m_∞	58.5	−23.66	−7.24
	h_∞		−52.43	8.48

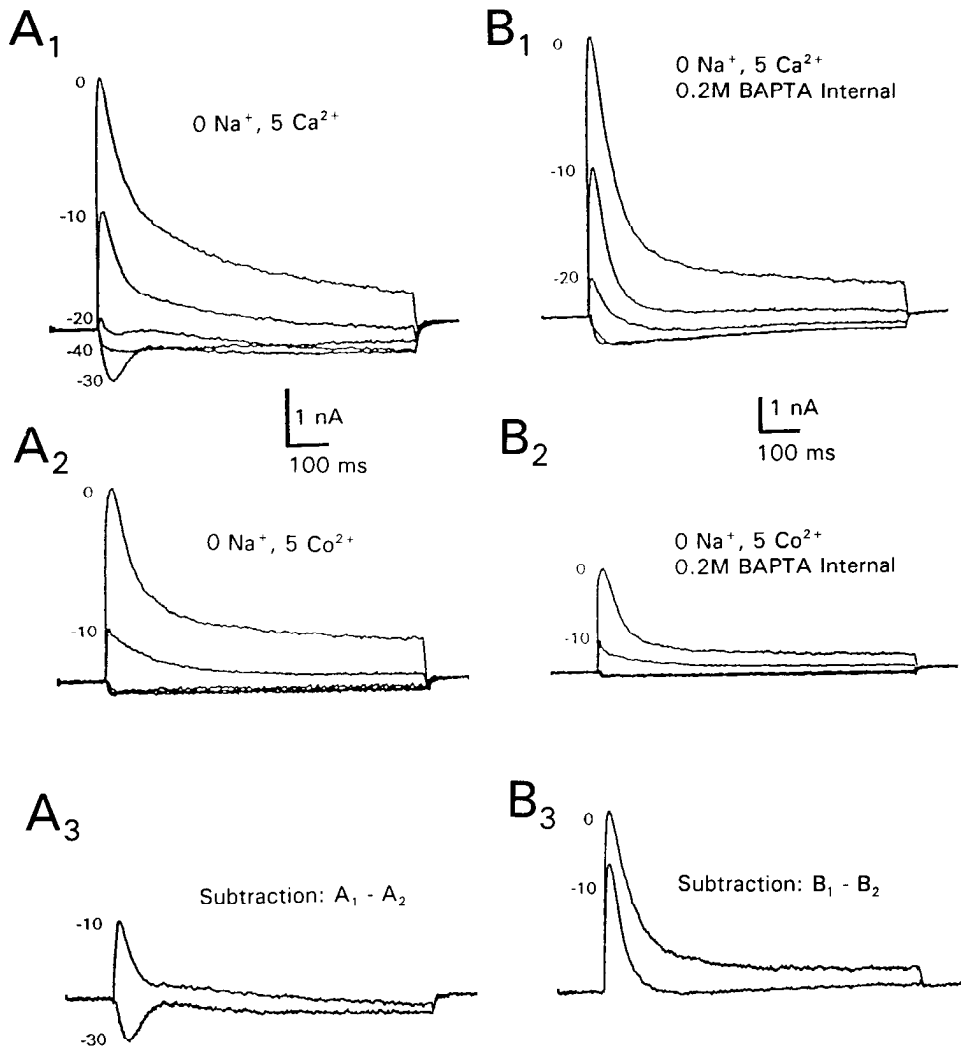

Figure 4. Calcium dependence of outward currents. Parts *A* and *B* were taken from different preparations. A_1, Currents obtained by step depolarizations to the potentials indicated from a holding potential of −70 mV in the presence of 5 mM external Ca^{2+}. A_2, Currents obtained by a voltage protocol similar to A_1 with 5 mM Co^{2+} replacing Ca^{2+}. A_3, Subtraction of the currents shown in A_2 from corresponding currents shown in A_1 to reveal at −30 mV an inward current carried by Ca^{2+} and at −10 mV an outward current dependent on Ca^{2+}. B_1, Currents obtained by step depolarizations to the potentials indicated from a holding potential of −70 mV in the presence of 5 mM external Ca^{2+} with BAPTA in the microelectrode. B_2, Currents obtained by a voltage protocol similar to B_1 with 5 mM Co^{2+} replacing Ca^{2+} with BAPTA in the microelectrode B_3, Subtraction of B_2 from B_1 revealing partial dependence of outward currents on internal [Ca^{2+}].

Steady state parameters of I_A

I_A was separated from I_K when currents obtained from a holding potential of −35 mV were subtracted from currents obtained from steps to identical voltages but from a holding potential of −70 mV (e.g., Fig. 1*A*). Figure 3*A* shows I_A activated by steps to −30 mV, −20 mV, −10 mV, and 0 mV. Conductance values were calculated based on a reversal potential of −75 mV (see Fig. 5). In a fashion similar to I_K, these values were converted to steady state activation by fitting to Equation 1 and dividing each value by G_{max} (Table 1). Steady state activation values were averaged (n = 6) and plotted versus membrane potential (Fig. 3*C*, open circles). The fit of Equation 1 with G_{max} taken as unity is also plotted (Fig. 3*C*, open circles). The fit of Equation 1 with G_{max} taken as unity is also plotted (Fig. 3*C*, line that follows open circles).

Steady state inactivation values for I_A were determined by maintaining the cell for 2 sec at different holding potentials and then stepping for 800 msec to a test potential of −20 mV (Fig. 3*B*). The holding potentials were increased in 5 mV increments from −90 mV to −25 mV in successive trials. Steady state inactivation was calculated as the ratio between the peak current obtained during the test pulse and the peak current from a holding potential of −90 mV. Steady state inactivation values were averaged (n = 5) and plotted (Fig. 3*C*, solid circles). Steady state inactivation for I_A was fit to Equation 1 using unity for G_{max} (Fig. 3*C*, line that follows open circles).

I_A started to activate at −45 mV and almost reached saturating conductance at 0 mV (Fig. 3*C*). Inactivation was about 90% removed at −70 mV, and 20% of the current remained at −40 mV. At −20 mV, I_A did not appear to inactivate completely, perhaps due to contamination by a slight amount of I_K.

Inactivation time constants for I_A varied between 89 ± 15 msec at −40 mV and 47 ± 1 msec at 0 mV (n = 8). The time constant for removal of inactivation of I_A was 35 ± 1 msec (n = 2).

Ca^{2+} dependence of outward currents

To test for the presence of Ca^{2+}-dependent outward currents, we looked for a difference in currents produced in the presence of 5 mM Ca^{2+} and when Ca^{2+} was replaced with Co^{2+} (Fig. 4*A*). I_A elicited by step depolarizations to −10 mV and 0 mV was slightly diminished by replacement of Ca^{2+}, while I_K was unaffected at these potentials (subtracted records, Fig. 4A_3). We obtained similar results in seven preparations.

The inward currents (Fig. 4A_1,A_3) observed in the presence of calcium appear due to the voltage-dependent Ca^{2+} currents found in leech heart interneurons (Angstadt and Calabrese, 1991).

We used BAPTA, a rapidly acting calcium chelator, in the microelectrodes to determine whether reduction of internal calcium could further reduce outward current. When BAPTA was used in the electrode and when external Ca^{2+} was replaced by Co^{2+}, there was a clear reduction of both I_A and I_K at steps to −10 mV and 0 mV (Fig. 4B_2). Subtraction of outward currents obtained from step depolarizations to −10 mV and 0 mV in 0 Na^+, 5 Co^{2+} saline from similar outward currents in 0 Na^+, 5 Ca^{2+} saline reveals the current blocked by Ca^{2+} substitution and internal BAPTA (Fig. 4B_3). We obtained similar results with BAPTA electrodes in seven preparations.

Reversal potential of I_K

We attempted to measure the reversal potential of I_K and to determine its dependence on external [K^+] using a modification of the method of reversal of tails. We were never able to observe a clear reversal of the tail current even at potentials down to −120 mV (not shown). Following a 75 msec activating prepulse to +20 mV from a holding potential of −35 mV (Fig. 5*A*), we stepped to a deactivating postpulse ranging from −25 mV to −65 mV. Both the amplitudes of currents during the activating prepulse and the tail currents (Fig. 5*B*) were larger in 1 mM [K^+] than in higher concentrations, as would be expected were K^+ the charge carrier for I_K. However, extrapolation of the amplitudes of tail currents in normal external [K^+] (4 mM) indicated a value for E_K of −55 mV to −65 mV, and there was only an 11 mV increase in the extrapolated reversal potential when external [K^+] was increased from 1 mM to 10 mM (not shown).

We felt this value for E_K was too positive (Nicholls and Kuffler, 1965; Deitmer and Schlue, 1981; Schlue et al., 1985), possibly because the amplitudes of the tails may be altered by capacitative current flow during the first 15 msec after stepping down or by the rapid deactivation of I_K at negative potentials. We chose the value of −75 mV for E_K for two reasons: (1) we saw only outward tail currents at −75 mV or more depolarized levels, and −75 mV was intermediate between our measurements and those measured previously as −80 mV (Deitmer and Schlue, 1981) and −83 mV to −89 mV (Nicholls and Kuffler, 1965).

The pharmacology of I_A *and* I_K *is consistent with their identity as* K^+ *currents*

After impaling heart interneurons with TEA-acetate electrodes, we observed spike broadening and reduction of the undershoot within 10 min after impalement, indicating that TEA was diffusing from the electrode. TEA blocked over 80% of I_A (Fig. 6*A,B*) and 90% of I_K (Fig. 6*C,D*). 4-AP at 5 mM added to the saline also reduced both I_A (Fig. 7*A,B*) and I_K (Fig. 7*C,D*). External TEA in concentrations up to 25 mM was not found to be effective in blocking K^+ currents in heart interneurons.

FMRF-NH_2 *shifts both activation and inactivation of* I_K

After 250 msec, I_A has inactivated to less than 10% of its peak amplitude, and hence, the magnitude of current at 250 msec (Fig. 1) is a measure of steady state activation of I_K from a holding potential of −70 mV. In the absence of FMRF-NH_2, I_K is initially activated at −20 mV when holding at −70 mV. When the peptide was bath applied, I_K was first activated at −30 mV and to a small extent at −40 mV (Fig. 1*A,B*; left). The average leak-subtracted total membrane current at 250 msec in the presence and absence of FMRF-NH_2 was compared at each test potential and was found to be significantly different at −40 mV, −30 mV, and −20 mV ($p < 0.05$, *t* test; $n = 7$) (see Fig. 9*A*), suggesting that FMRF-NH_2 causes a negative shift in the *I/V* relation and thus steady state activation of I_K.

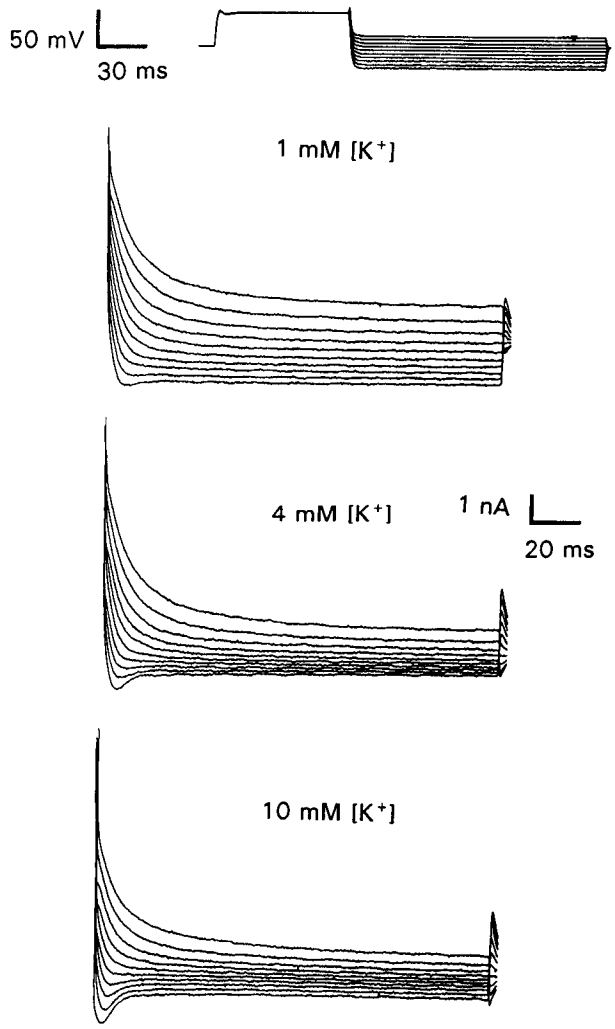

Figure 5. Reversal potential of I_k. The *upper panel* shows the deactivation protocol used to elicit tail currents. Tail currents were obtained by stepping to +20 mV for 75 msec and deactivating at potentials between −65 mV and −25 mV. The *three lower panels* show tail currents during the deactivation postpulse from a single heart interneuron in three different external [K^+].

We used a standard inactivation voltage protocol to measure steady state inactivation of I_K in the absence (Fig. 8*A*) and presence (Fig. 8*B*) of FMRF-NH_2. The average steady state inactivation (I/I_{max} at 250 msec) was compared at each value of holding potential and found to be significantly different at −50 mV, −40 mV, and −30 mV ($p < 0.05$, *t* test; $n = 8$) (Fig. 9*B*). These findings suggest that FMRF-NH_2 causes a negative shift in steady state inactivation. The increment in steady state inactivation at −35 mV can explain the paradoxical reduction of I_K by FMRF-NH_2 when elicited from this holding potential (compare Fig. 1*A,B*; right panels).

Time constants for activation, deactivation, and inactivation of I_K *are unchanged by FMRF-*NH_2

We measured activation time constants for I_K in the presence and absence of FMRF-NH_2. Activation time constants were measured from currents in response to brief (120 msec) depo-

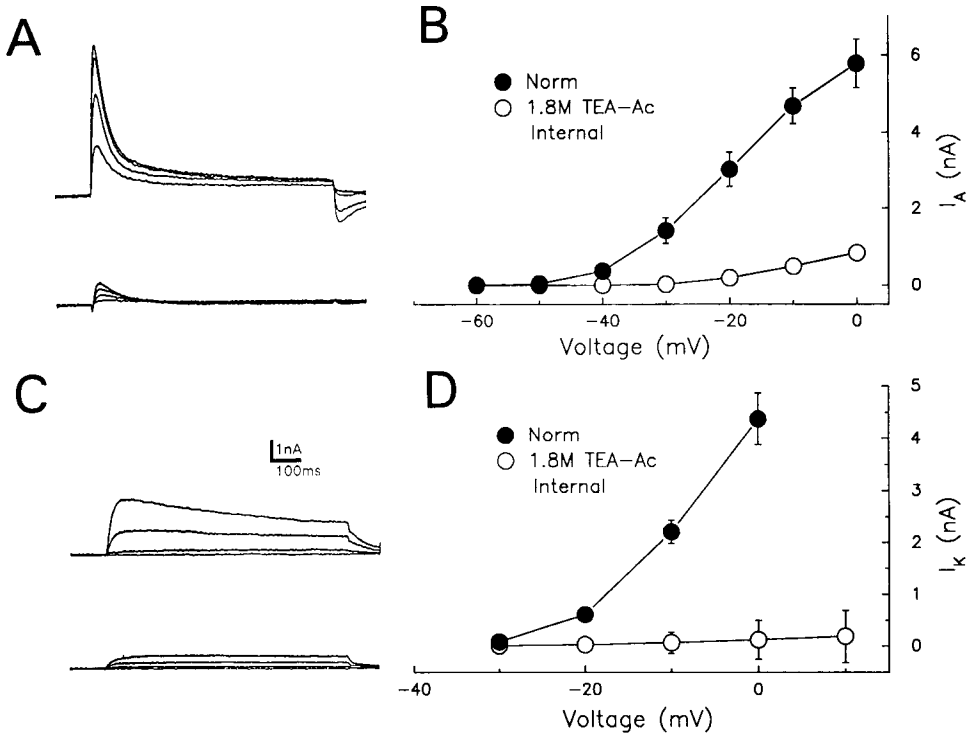

Figure 6. Effect of TEA on I_A and I_K. *A*, Reduction of I_A by internal TEA. *Top*, Representative I_A at −30 mV, −20 mV, −10 mV, − 10 mV determined by subtraction (compare Fig. 3*A*). *Bottom*, I_A measured in a similar way with a TEA electrode. *B*, Current–voltage relation for peak current elicited from a holding potential of −70 mV with (*open circles*; n = 10) and without (*solid circles*; n = 16) TEA in the electrode. *C*, Reduction of I_K by internal TEA. *Top*, Representative I_K at −30 mV, −20 mV, −10 mV, and 0 mV. *Bottom*, I_K measured similarly with a TEA electrode. *D*, Current–voltage relation for peak current elicited from a holding potential of −35 mV with (*open circles*; n = 10) and without (*solid circles*; n = 16) TEA in the electrode. All points in *B* and *D* are means ± SEM.

larizing pulses (Fig. 10*A*) with the assumption that the underlying conductance activated via a second-order power function (Johansen and Kleinhaus, 1986). In the same preparation, deactivation time constants were measured during a postpulse at a range of membrane potentials following a 75 msec activating prepulse (Fig. 10*B*). Currents used to measure deactivation time constants were corrected by subtracting the current measured during a hyperpolarizing pulse of equal magnitude (see Materials and Methods) to remove the capacitative and the passive leakage currents. We were not confident that we could measure the activation time constants with complete accuracy because of the settling time of the electrode and because during large depolarizing steps, voltage control in our experiments was not established for at least 5–10 msec (e.g., voltage traces in Fig. 10*A*). The settling time of the electrode was similar whether FMRF-NH_2 was present or not, and we kept the switching frequency

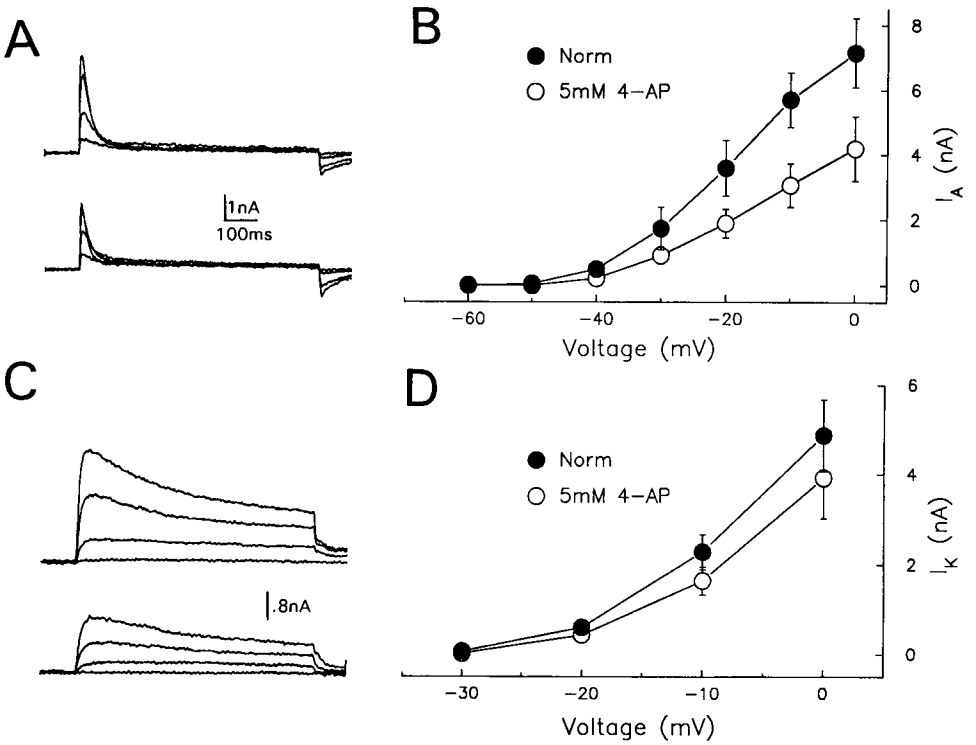

Figure 7. Effect of 4-AP on I_A and I_K. *A*, Reduction of I_A by external 4-AP. *Top*, Typical I_A measured by subtraction (compare Fig. 3*A*) at −30 mV, −20 mV, −10 mV, and 0 mV from a holding potential of −70 mV before addition of 5 mM 4-AP to the saline. *Bottom*, Similar currents from the same neuron after addition of 5 mM 4-AP to the saline. *B*, Current–voltage relation for I_A with (*open circles*) and without (*solid circles*) 5 mM 4-AP (n = 6). *C*, Reduction of I_K by external 4-AP. *Top*, Typical I_K obtained by stepping to −30 mV, −20 mV, −10 mV, and 0 mV from a holding potential of −35 mV without 4-AP. *Bottom*, Similar currents from the same neuron after addition of 5 mM 4-AP. *D*, Current–voltage relation for I_K with (*open circles*) and without (*solid circles*) 5 mM 4-AP (n = 6). All points in *B* and *D* are means ± SEM.

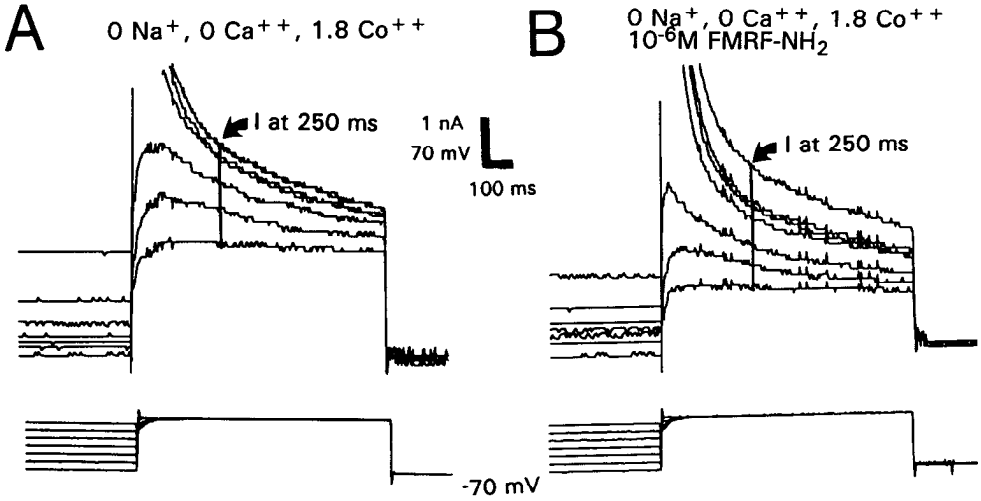

Figure 8. Effect of $FMRF\text{-}NH_2$ on steady state inactivation of I_K. Outward currents recorded during a test pulse of an inactivation protocol in the absence (*A*) and presence (*B*) of 10^{-6} M $FMRF\text{-}NH_2$. Holding potentials varied from −70 mV to 0 mV, and the test pulse was to 0 mV. In order to insure that the I_K measurement was not contaminated by residual I_A, currents were measured at 250 msec, similar to Figure 1. The inactivation prepulse was 2.5 sec, and the test pulse was 800 msec.

of the voltage clamp above a minimum of 5 kHz (recording bandwidth, 1 kHz), theoretically allowing us to measure accurately a time constant of 5 msec. We measured time constants from currents elicited by voltage steps to +5 mV or less because at higher potentials, our inability to establish voltage control rapidly enough could cause us to underestimate the activation time constant.

Average results at each test potential for activation time constants were compared and found to be similar whether $FMRF\text{-}NH_2$ was present or not ($p > 0.6$, t test; $n = 5$) (Fig. 10*C*). Average results at each postpulse potential for deactivation time constants were compared and also found to be similar whether $FMRF\text{-}NH_2$ was present or not ($p > 0.4$, t test; $n = 9$) (Fig. 10*D*).

I_K inactivated with a single exponential time course in the presence or absence of $FMRF\text{-}NH_2$ (Fig. 11*A*). Inactivation time constants were measured from currents evoked by step depolarizations from a holding potential of −35 mV (Fig. 11*B*). Averages of the inactivation time constants were compared at each test potential, and no significant differences in the presence or absence of $FMRF\text{-}NH_2$ were found ($p > 0.6$, t test; $n = 7$) (Fig. 11*C*).

Both TEA and 4-AP interfere with the effects of $FMRF\text{-}NH_2$ on I_K

We examined the effects of TEA and 4-AP on the ability of $FMRF\text{-}NH_2$ to alter I_K observed at a holding potential of −35 mV. When using TEA-containing electrodes, no $FMRF\text{-}NH_2$-induced reduction of I_K was observed.

We added 5 mM 4-AP in 0 Na^+, 0 Ca^{2+}, 1.8 Co^{2+} saline and also did not observe the characteristic $FMRF\text{-}NH_2$-induced reduction of I_K from a holding potential of −35 mV.

Hodgkin–Huxley models of I_A and I_K

A goal of this investigation was to provide quantitative models of the outward currents for use in future network simulations. We used Hodgkin–Huxley kinetic models of I_A and I_K with rate constants describing state transitions that were functions of membrane potential (Hodgkin and Huxley, 1952b; Beeler and Reuter, 1977; Yamada et al., 1989). Both I_K and I_A could be well represented by

$$I = G_{max} m^2(V, t) h(V, t)(V - E_K). \quad (3)$$

The equation for the rate constants underlying kinetic param-

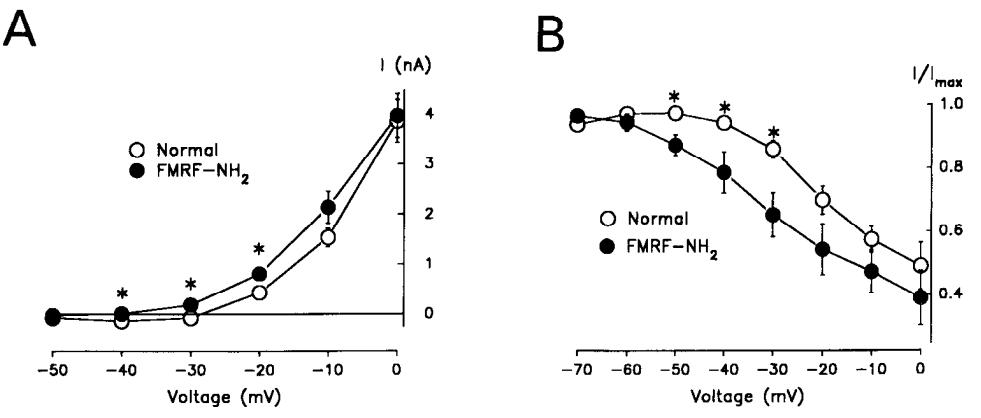

Figure 9. $FMRF\text{-}NH_2$-induced hyperpolarizing shifts in steady state activation and inactivation of I_K. *A*, Current–voltage relationship for leak-subtracted total membrane current elicited from −70 mV measured at 250 msec from the start of the step in the presence (*solid circles*) and absence (*open circles*) of 10^{-6} M $FMRF\text{-}NH_2$ (means ± SEM). *Asterisks* indicate values that are significantly different at the 5% level (t test; $n = 7$). *B*, Steady state inactivation of I_K measured at 250 msec (Fig. 8) in the presence (*solid circles*) and absence (*open circles*) of 10^{-6} M $FMRF\text{-}NH_2$) (means ± SEM). *Asterisks* indicate values that are significantly different at the 5% level (t test; $n = 8$).

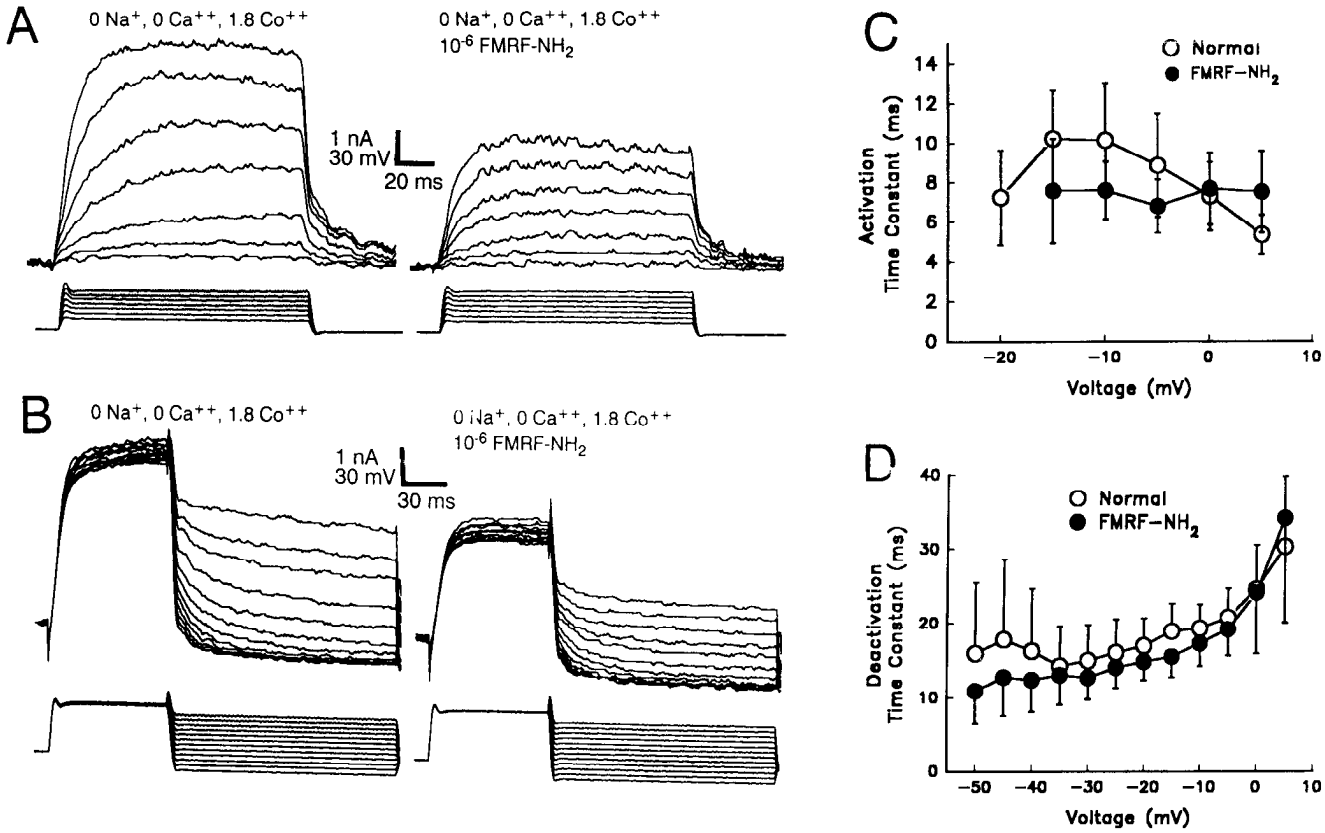

Figure 10. Activation and deactivation time constants for I_K. *A*, Example of currents used to measure activation time constants in the absence (*left*) and presence (*right*) of 10^{-6} M FMRF-NH_2. I_K was elicited by step depolarizations to −25, −20, −15, −10, −5, 0, and +5 mV from −35 mV. *B*, Example of currents used to measure deactivation time constants in the absence (*left*) and presence (*right*) to 10^{-6} M FMRF-NH_2. Following a step to +20 mV, deactivation was measured during a postpulse to potentials that ranged from +10 to −50 mV. *C*, Plot of average activation time constants versus membrane potential in the presence (*solid circles*) and absence (*open circles*) of 10^{-6} M FMRF-NH_2 (means ± SEM; $n = 5$). *D*, Plot of average deactivation time constants versus membrane potential in the presence (*solid circles*) and absence (*open circles*) of 10^{-6} M FMRF-NH_2 (means ± SEM; $n = 9$).

eters, m and h, and the numerical values used are listed in Table 2.

We split I_K into two components: a rapid-onset, inactivating conductance termed the "fast" component or I_{KF} and a slower-onset, noninactivating conductance, the "slow" component or I_{KS}. FMRF-NH_2 shifted the activation of both I_{KF} and I_{KS}, and shifted the inactivation of I_{KF}.

There are three reasons to divide I_K into these two components. First, about 30% of I_K remained after an inactivating prepulse to 0 mV (Figs. 2*B,C*; 8; 9*B*); this 30% is assumed to

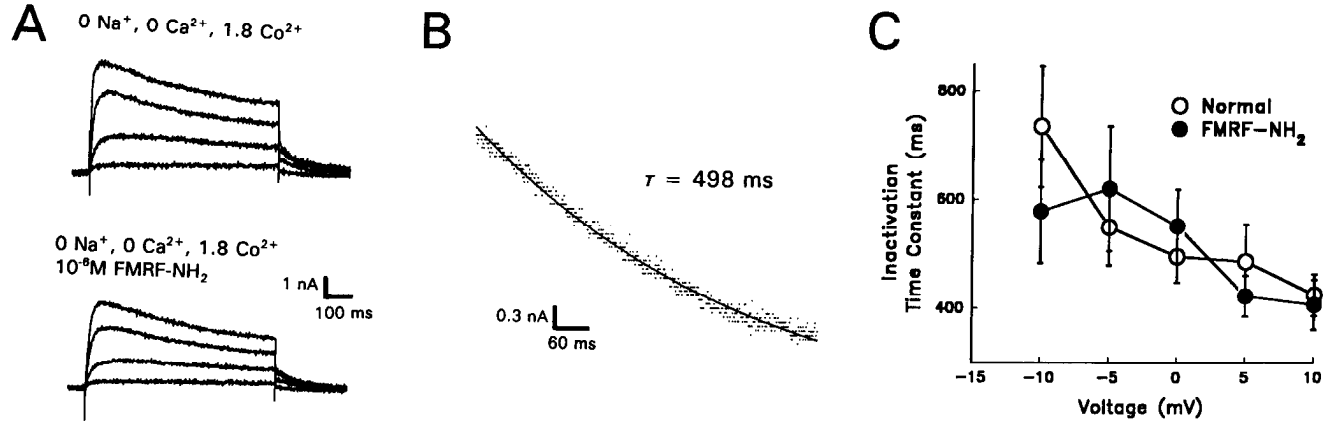

Figure 11. Inactivation time constants of I_K. *A*, An example of currents evoked from a holding potential of −35 mV in the absence (*upper*) and presence (*lower*) of 10^{-6} M FMRF-NH_2. *B*, Single exponential fit of the time course of inactivation of the current in *A* evoked by a step to +5 mV. *C*, Plot of average inactivation time constants versus voltage in the presence (*solid circles*) and absence (*open circles*) of 10^{-6} M FMRF-NH_2 (means ± SEM; $n = 7$).

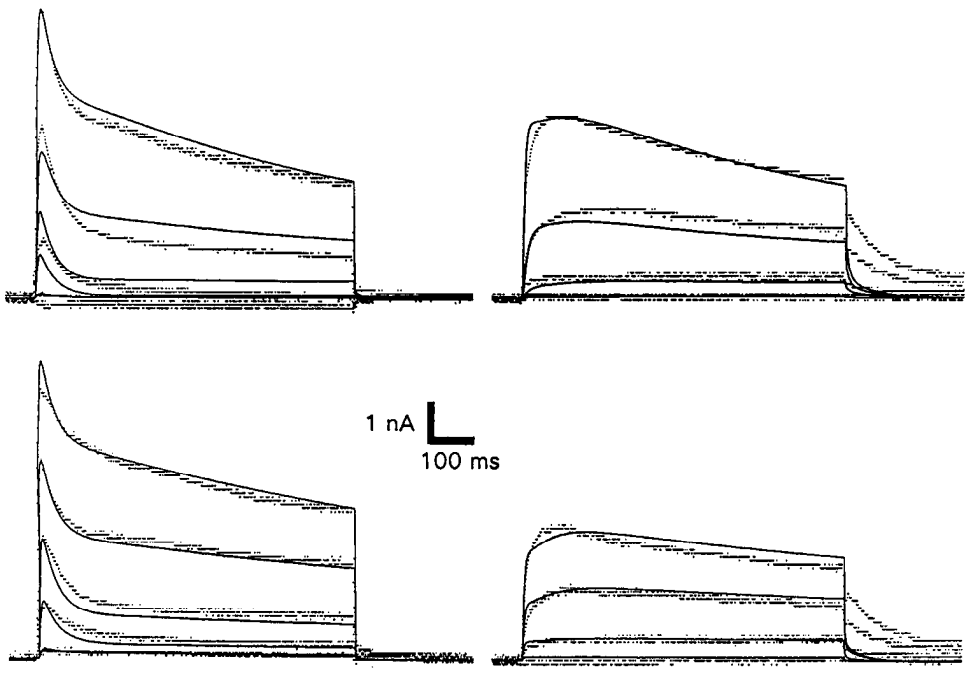

Figure 12. Simulation of the effect of FMRF-NH_2 on I_K. Results of the simulation (*smooth lines*) are displayed over the data points from Figure 1. See text for details.

be I_{KS}. Second, the time course of inactivation of I_K was extremely well fit by a single exponential (Fig. 11*B*), and initial simulations with only a single type of conductance inactivated to a greater extent (i.e., less current) at the end of an 800 msec test pulse than did the actual data. (e.g., Figs. 1, 2*A*). Third, previous workers have also found a noninactivating fraction of I_K in frog myelinated nerve (Schwarz and Vogel, 1971).

Activation rate constants for I_{KF} were first calculated using steady state activation values (Figs. 1, 9) and activation time constants (Fig. 10). Inactivation rate constants for I_{KF} were calculated using steady state inactivation values (Figs. 8, 9) and inactivation time constants (Fig. 11).

Activation rate constants for I_{KS} were calculated assuming that steady state activation of I_{KS} was the same as that for I_{KF} and estimating activation time constants of I_{KS} as one-third of the time to peak after the start of depolarizing pulses from −35 mV (e.g., Figs. 1*A,B*, right panels; 2*A*).

The activation rate constants for I_A were calculated using measured steady state values (Fig. 3*C*) and assuming a voltage-independent activation time constant of 3 msec, similar to the value measured in the leech *Macrobdella decora* (Johansen and Kleinhaus, 1986). Inactivation rate constants for I_A were calculated using steady state values (Fig. 3*B,C*) and time constants measured from these same data during the first 200–250 msec following the peak. Inactivation time constants were quite variable between experiments. They were fit well by a single exponential and decreased with depolarization.

Maximum conductances (G_{max}) for I_A and I_K in the simulation were taken to be the parameters determined by fitting steady state values to Equation 1 (Table 1). The reversal potential of potassium was assumed to be −75 mV (see Fig. 5 and above).

Equations for the dependence of the rate constants on membrane potential were determined by fitting to Equation 4 (Table 2). Simulations of voltage-clamp experiments (e.g., Fig. 1) were performed with these rate constant expressions. We compared the results of the simulation with the data (Fig. 1) and iteratively adjusted the numerical values of the rate constants until the results of the simulation were satisfactory (Fig. 12). We further checked the simulation by calculating steady state activation and inactivation and accompanying time constants for the various model currents and found they were in good agreement with the data (not shown).

Table 2. Constants used to calculate rate constants of the Hodgkin-Huxley models of I_A and I_K.

Rate constant		P_1	P_2	P_3	P_4
I_A	α_{mA}	0.335	−0.13	32.5	0.86
	β_{mA}	2.48	0.12	50	7.5
	α_{hA}	0.03	0.236	50	1
	β_{hA}	0.029	−0.20	56	1
Normal					
I_{KF}	α_{mKF}	1	−0.13	−10	1
	β_{mKF}	1	0.035	72	8.5
	α_{hKF}	0.002	0.11	19	1
	β_{hKF}	0.00144	−0.2	24	1
I_{KS}	α_{mKS}	0.2	−0.17	2	20
	β_{mKS}	0.2	0.15	15	20
FMRF-NH_2					
I_{KF}	α_{mKF}	1	−0.04	−25	1
	β_{mKF}	1	0.12	28	4
	α_{hKF}	0.0006	0.06	25	1
	β_{hKF}	0.0009	−0.06	30	1
I_{KS}	α_{mKS}	0.25	−0.2	1	20
	β_{mKS}	0.25	0.04	40	20

The generalized Boltzmann-type equation used to describe the dependence of the rate constants, α and β, on membrane potential was taken from Beeler and Reuter (1977): rate $(V) = P_1/(e^{P_2 \cdot (V+P_3)} + P_4)$. The constants P_1–P_4 are given above.

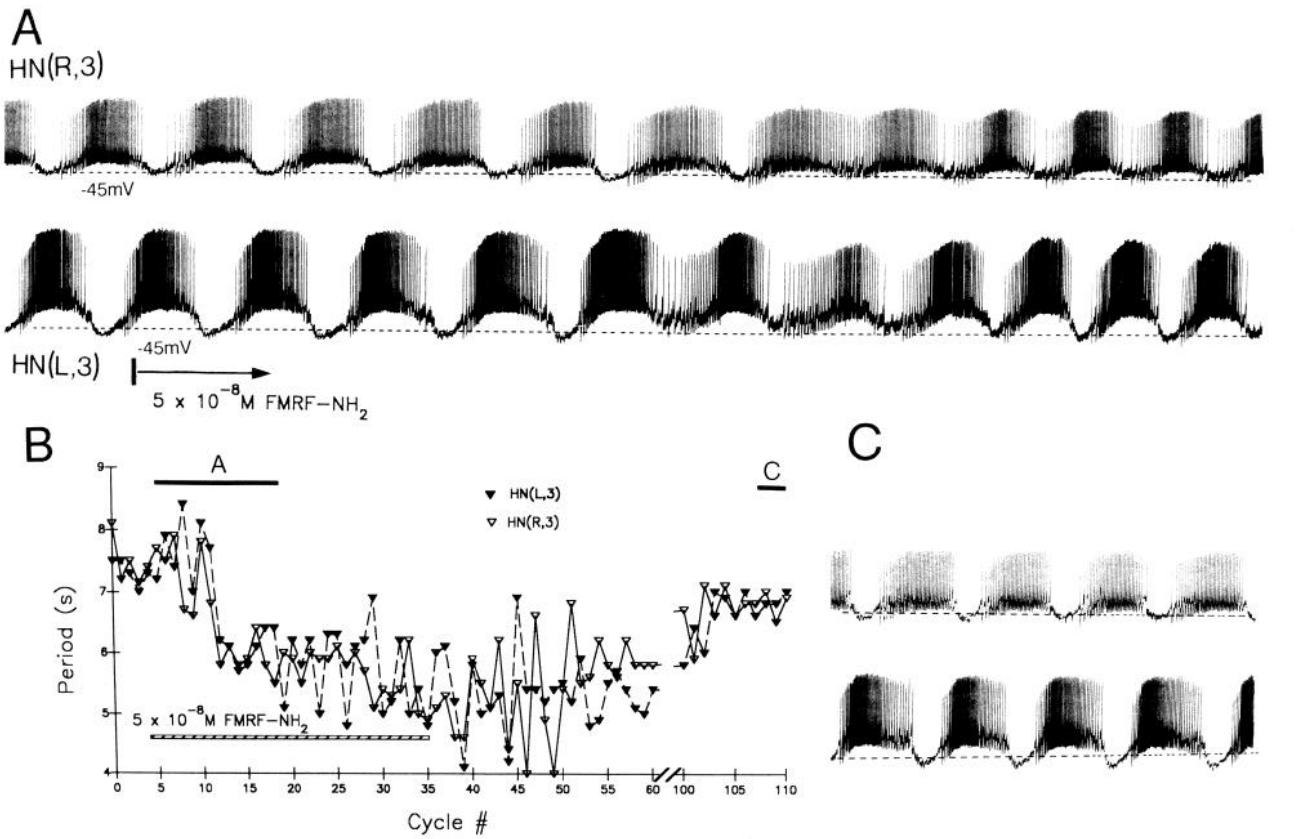

Figure 13. Acceleration of the heart rate in an oscillatory pair of heart interneurons in response to bath application of 5×10^{-8} M FMRF-NH_2. *A*, Membrane potential recording from both heart interneurons in ganglion 3 as the FMRF-NH_2 takes effect. Note the reduction in cycle period. *B*, Plots of cycle period in both heart interneurons versus cycle number (#). Cycle numbers were incremented from 0 starting three cycles before addition of 5×10^{-8} M FMRF-NH_2 to the bath. The *bars* labeled *A* and *C* above the plots indicate the sections of this graph corresponding to parts *A* and *C* of this figure. *C*, Recording from the same neurons about 5 min after washing out the FMRF-NH_2.

FMRF-NH_2 can cause either acceleration of the cycle rate or disruption of the rhythm of heart interneurons

We wished to examine the effects of bath-applied FMRF-NH_2 on the oscillatory activity of the heart interneurons with the hope that modulation of I_K might provide a mechanism for these effects. Bath application of FMRF-NH_2 produced an increase in the cycle rate of leech heart interneurons (Fig. 13*A*). A concentration of 5×10^{-8} M FMRF-NH_2 reduced the period from 7.5–8.5 sec to about 6 sec (Fig. 13*B*). The acceleration of the rhythm could be reversed by washing out the FMRF-NH_2, and in this preparation, the period increased to about 7 sec after a 5 min wash (Fig. 13*C*). As the FMRF-NH_2 entered the bath, a large amount of variability of the cycle period was evident (Fig. 13*A,B*). Variability in the cycle period also occurred during washout of FMRF-NH_2. This variability may possibly be due to a disruptive effect of FMRF-NH_2.

This disruptive effect of FMRF-NH_2 (Fig. 14) often results in an arrhythmic episode. During such as episode, the neurons assume a potential very near the level that they attain during their bursting phase, approximately −30 to −35 mV. It appears that the inability of one heart interneuron to silence effectively the activity of the other through synaptic inhibition has been reduced. However, no apparent effect of FMRF-NH_2 on graded synaptic transmission under presynaptic voltage clamp was observed by Angstadt and Calabrese (1991).

We recorded from at least one member of eight pairs of reciprocally inhibitory heart interneurons (third and fourth ganglia) during exposure to 5×10^{-8} M FMRF-NH_2. In five preparations, we observed an increase in the cycling rate, and in the remaining three, a disruption of the rhythm. We exposed five other similar preparations to 1×10^{-6} M FMRF-NH_2, and four showed a disruption of the rhythm. The fifth preparation showed a transient disruption of 30–40 sec followed by an increase in cycle rate.

Discussion

The ionic basis of outward currents in heart interneurons

The identification of I_K as a potassium current is supported by its dependence on external [K^+] (Fig. 5). Only chloride and potassium have reversal potentials close to our measurement of that for I_K. The fact that both TEA and 4-AP reduce I_A and I_K is also strongly suggestive of their identification as potassium currents (Figs. 6, 7).

We observe an 11 mV shift in E_K for a 10-fold change in external [K^+]. One possible mechanism to account for this smaller than predicted shift is regulation of internal potassium concentration or activity. Changes in the internal K^+ activity of leech R cells have been observed in response to changes in external [K^+] (Deitmer and Schlue, 1981).

We were able to raise external [K^+] to only 10 mM because higher concentrations depolarized and subsequently killed the

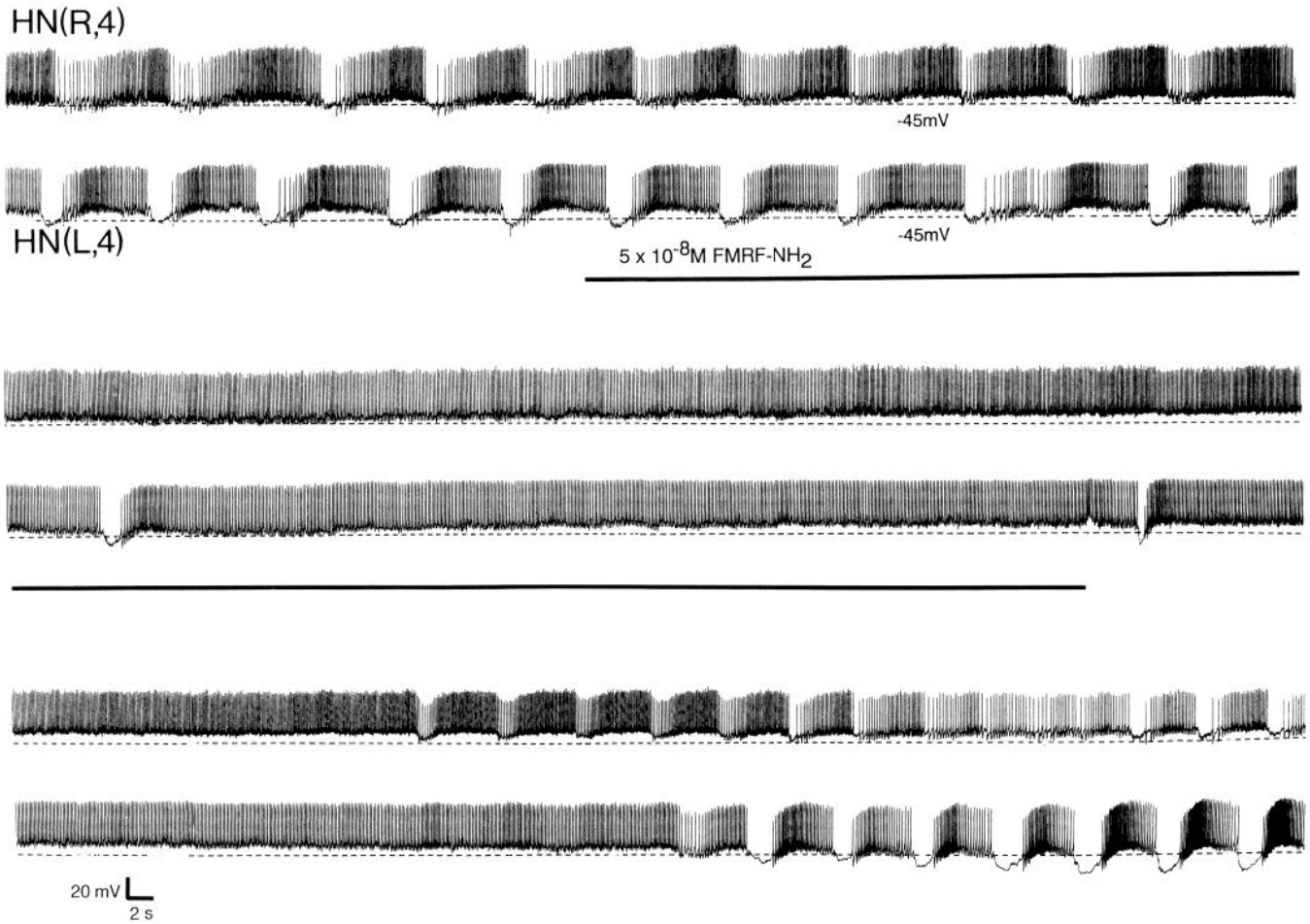

Figure 14. FMRF-NH_2-induced disruption of rhythmic activity in the oscillatory pair of heart interneurons in ganglion 4. The three traces are a continuous record. FMRF-NH_2 (5×10^{-8} M) was bath applied during the period of time marked with the *solid line* below the pair of voltage recordings. The *broken lines* immediately below each voltage trace represent a membrane potential of −45 mV. Rhythmic activity was restored by washing out the FMRF-NH_2.

heart interneurons. Based on an internal K^+ concentration of 135 mM (Dietmer and Schlue, 1981), the predicted potassium reversal potential in 10 mM external [K^+] is −66 mV, and we could not observe a tail reversal even at postpulses below −90 mV. In 40 mM external [K^+] used in another study (Stewart et al., 1989), the predicted potassium reversal potential is −27 mV, and it was possible to inward tail currents following a depolarization.

Adequacy of voltage control and space clamp

Voltage control over the outward currents in heart interneurons was generally good. However during the first 10–20 msec of large step depolarizations, the electrode could not inject enough current to maintain a stable command voltage in the cell soma (e.g., Fig. 1). Hence, to reduce error in computing peak current values, we restricted the range of step depolarizations to 0 mV when holding at −70 mV, and to +15 mV when holding at −35 mV (e.g., Figs. 2, 3). To reduce error when computing activation time constants of I_K, we restricted this range to + 5 mV.

There are three reasons to believe we have good voltage control not only of the cell soma but also of the dendritic processes of the heart interneurons. First, input resistance of the cells in successful experiments was high—60–80 MΩ. Second, we have eliminated inward currents by recording in Na^+- and Ca^{2+}-free saline, thus greatly reducing the increase in conductance due to depolarizing voltage steps. Third, contacts with other heart interneurons occur at only the distal tips of the dendrites (Tolbert and Calabrese, 1985), and presumably Cl^--mediated IPSPs also originate at these distal tips. Because IPSPs can be reversed by current injection at the soma (Angstadt and Calabrese, 1991), we assume that the heart interneurons are electrically compact.

Accuracy of the Hodgkin–Huxley model of outward currents

We developed the model of I_A and I_K for use in network simulations (e.g., DeSchutter et al., 1992). As a starting point, we used the averaged data from several successful preparations and then refined the model until it closely matched one experiment (Figs. 1, 12). When time constants and steady state values for both I_K and I_A were calculated from the rate constants (Table 2), they matched the averaged data quite well. The model clearly recreates the paradoxical effect of FMRF-NH_2 on I_K produced by the negative shifts in activation and inactivation, and it will be useful in future simulations (e.g., DeSchutter et al., 1992).

The model does fail to reproduce the tail currents observed upon deactivation of I_K to −35 mV (Fig. 12). This suggests that

I_K includes several components that differ in their kinetic properties (e.g., Dubois, 1981). One explanation for the failure of the model to reproduce the tail currents is that I_K includes a component that activates and deactivates very slowly, similar to I_{K2} in cultured leech neurons (Stewart et al., 1989). Another explanation is that deactivation of I_K occurs by a different process than its activation, in a manner antithetical to the classical mechanism (Hodgkin and Huxley, 1952b).

Ca^{2+} dependence of outward currents?

There does not appear to be an I_c or slowly activating Ca^{2+}-dependent potassium current (Meech and Standen, 1975; Thompson, 1977) in heart interneurons as occurs in cultured leech R neurons (Stewart et al., 1989). A portion of I_A may depend on calcium influx (Fig. $4A_3$). This dependence might reflect a Ca^{2+}-activated fast potassium current similar to that found in *Aplysia* neurons (Junge, 1985), calf cardiac Purkinje fibers (Siegelbaum and Tsien, 1980), and bullfrog sympathetic neurons (MacDermott and Weight, 1982). Both removal of external Ca^{2+} and an internal Ca^{2+} chelator produced a decrease in I_K (Fig. $4B_3$). Thus, Ca^{2+} may enhance activation of both I_K and I_A. In squid axon, Ca^{2+} is needed for complete activation of K^+ channels (Armstrong and Lopez-Barneo, 1987), and in a heterologous expression system, Shaker A-type K^+ channels also required Ca^{2+} (Armstrong and Miller, 1990).

Comparison of outward currents in heart interneurons with those in other leech neurons

Three potassium currents, I_A, I_K, and a calcium-activated K^+ current, I_c, have been found in cultured AP, R, N, P, and T cells, but not all currents are found in each cell type (Stewart et al., 1989; Garcia et al., 1990). I_A is present in AP and R cells, and in AP cells, its inactivation kinetics appear similar to those in heart interneurons. In contrast with heart interneurons, a major portion of the voltage-dependent potassium conductance in cultured R cells is I_c. Similar to heart interneurons, cultured P, T, N, and R cells contain two components of I_K, distinguishable by their fast and slow kinetics (Stewart et al., 1989).

Johansen and Kleinhaus (1986) investigated I_A and I_K in R cell somata of the leech *Macrobdella decora*. I_A in R cell somata had a slightly higher threshold than I_A in heart interneurons, and I_K in these cells inactivated more slowly than I_{KF} in heart interneurons.

Comparison of the effect of FMRF-NH_2 on I_K in leech heart interneurons with other modulated currents

Voltage shifts in kinetic properties of I_K and other currents have been observed elsewhere. In bullfrog atrial myocytes, activation of the delayed rectifier is shifted to more negative potentials by cAMP, norepinephrine (Tsien et al., 1972), isoprenaline (Giles et al., 1989), or forskolin (Duchatelle-Gourdon et al., 1989), and the time course of activation is more rapid. In squid giant axon, both activation and inactivation of I_K were shifted to more depolarized potentials by internal dialysis of ATP, presumably by phosphorylation of the K-channel protein by membrane-bound kinases and a subsequent change in the electric field around the channel's voltage sensor (Bezanilla et al., 1986). In pleural sensory neurons of *Aplysia*, 5-HT may also cause a shift in the voltage dependence of activation and inactivation of I_K and affected time constants of both processes (Baxter and Byrne, 1989). Internal perfusion of the squid giant axon with arachidonic acid caused a positive shift in fast Na^+ current activation (Takenaka et al., 1988). In leech R cells, 5-HT enhanced the peak amplitude of I_A and increased its inactivation time constant, and, similar to the effect of FMRF-NH_2 in heart interneurons 5-HT reduced the amplitude of I_K evoked by depolarizations from −30 mV (Acosta-Urquidi et al., 1989).

In all these examples, the changes in steady state parameters and/or time constants can be explained by a shift in the voltage dependence of the Hodgkin–Huxley rate constants, and these shifts may be a common mechanism of modulation of voltage-gated conductances. Apparently, FMRF-NH_2 modulation of I_K in leech heart interneurons occurs solely by a shift in steady state activation and inactivation; within the resolution of our measurement system, the time constants are unaffected.

Function of I_K in the heart interneuron cycle

One function of I_K in heart interneurons appears to be repolarization of spikes (cf. Rudy, 1988). The falling phase of spikes in the middle and late parts of a burst occurs via I_K. The falling phase of the three to four spikes prior to a plateau/burst (Fig. 13*A*) includes a large undershoot, suggesting that both I_A and I_K serve to repolarize these initial spikes. I_K may also function to modulate both graded and spike-mediated transmission (see below).

Modulation of I_K suggests a possible basis for both the acceleratory and the disruptive effect of FMRF-NH_2 on the rhythm

Interaction between I_K and processes underlying spike-mediated transmission, acting through the membrane potential, suggests an explanation for the acceleratory effects of FMRF-NH_2 on the heart rhythm. During the plateau/burst phase, spikes arise from a potential of −35 mV to −40 mV, a polarization level at which the inactivation shift of FMRF-NH_2 would exert a large effect to reduce the magnitude of I_K. This suggests that at these relatively depolarized levels, one might observe FMRF-NH_2-induced spike broadening and, in consequence, increased spike-mediated transmission. Consistent with this explanation is the presence of prominent spike-mediated IPSPs during the FMRF-NH_2-induced acceleratory response (Fig. 13*A*). The increased transmission would enhance I_h (Angstadt and Calabrese, 1989) in the inhibited cell, and escape from inhibition (Calabrese et al., 1989) would occur more quickly.

Interaction between I_K and the calcium currents underlying graded synaptic transmission, again, mediated by the membrane potential, suggests an explanation for the disruptive effects of FMRF-NH_2 (Fig. 14). During the early part of a burst, spikes arise from a relatively hyperpolarized membrane potential (−60 mV to −50 mV), and in the presence of FMRF-NH_2, there would be increased activation of I_K (compare Figs. 1, 9*A*) with no effect or minimal effect of the inactivation shift of I_K. A larger I_K would be expected to mitigate I_{Ca} underlying graded transmission by interaction through the membrane potential (cf. Angstadt and Calabrese, 1991). Consistent with this rationale is the fact that the inhibitory troughs in an acceleratory response are less hyperpolarized in FMRF-NH_2 than in its absence (Fig. 13*A*).

The interplay between the activation shift and the inactivation shift of I_K by FMRF-NH_2 determines the variability of the responses we have observed.

References

Acosta-Urquidi J, Sahley CL, Kleinhaus AL (1989) Serotonin differentially modulates two K^+ currents in the Retzius cell of the leech. J Exp Biol 145:403–417.

Aghajanian GK (1985) Modulation of a transient outward current in serotonergic neurones by α_1-adrenoceptors. Nature 315:501–503.

Angstadt JD, Calabrese RL (1989) A hyperpolarization-activated inward current in heart interneurons of the medicinal leech. J Neurosci 9:2846–2857.

Angstadt JD, Calabrese RL (1991) Calcium currents and graded synaptic transmission between heart interneurons of the leech. J Neurosci 11:746–759.

Arbas EA, Calabrese RL (1984) Rate modification in the heartbeat central pattern generator of the medicinal leech. J Comp Physiol A 155:784–794.

Armstrong CM, Lopez-Barneo J (1987) External calcium ions are required for potassium channel gating in squid neurons. Science 236: 712–714.

Armstrong CM, Miller C (1990) Do voltage-dependent K^+ channels require Ca^{2+}? A critical test employing a heterologous expression system. Proc Natl Acad Sci USA 88:652–656.

Baxter DA, Byrne JH (1989) Serotonergic modulation of two potassium currents in the pleural sensory neurons of *Aplysia*. J Neurophysiol 62:665–679.

Beeler GW, Reuter H (1977) Reconstruction of the action potential of ventricular myocardial fibres. J Physiol (Lond) 268:177–210.

Bezanilla F, Caputo C, DiPolo R, Rojas H (1986) Potassium conductance of the squid giant axon is modulated by ATP. Proc Natl Acad Sci USA 83:2743–2745.

Calabrese RL (1977) The neural control of alternate heartbeat coordination states in the leech, *Hirudo medicinalis*. J Comp Physiol 122: 111–143.

Calabrese RL, Angstadt JD, Arbas EA (1989) A neural oscillator based on reciprocal inhibition. In: Perspectives in neural systems and behavior (Carew TJ, Kelley DB, eds), pp 33–50. New York: Liss.

Connor JA, Stevens CF (1971) Voltage clamp studies of a transient outward current in gastropod neural somata. J Physiol (Lond) 213: 1–19.

DeFelice LJ, Goolsby W, Huang D (1985) Membrane noise and excitability. In: Noise in physical systems and 1/f noise (D'Amico A, Mazzetti P, eds), pp 35–45. Amsterdam: Elsevier.

Deitmer JW, Schlue WR (1981) Measurements of the intracellular potassium activity of Retzius cells in the leech central nervous system. J Exp Biol 91:87–101.

DeSchutter E, Simon TW, Angstadt JD, Calabrese RL (1992) Modeling a neural oscillator that paces heartbeat in the medicinal leech. Am Zool, in press.

Dubois JM (1981) Evidence for the existence of three types of potassium channels in the frog Ranvier node membrane. J Physiol (Lond) 318:297–316.

Duchatelle-Gourdon I, Hartzell HC, LaGrutta AA (1989) Modulation of the delayed rectifier potassium current in frog cardiomyocytes by β-adrenergic agonists and magnesium. J Physiol (Lond) 415:251–274.

Garcia R, Grumbacher-Reinert S, Bookman R, Reuter H (1990) Distribution of Na^+ and K^+ currents in soma, axons and growth cones of leech Retzius neurons in culture. J Exp Biol 150:1–17.

Giles W, Nakajima T, Ono K, Shibata EF (1989) Modulation of the delayed rectifier K^+ current by isoprenaline in bull-frog atrial myocytes. J Physiol (Lond) 415:233–249.

Harris-Warwick R, Flamm RE (1987) Multiple mechanisms of bursting in a conditional bursting neuron. J Neurosci 7:2113–2128.

Hodgkin AL, Huxley AF (1952a) Currents carried by sodium and potassium ions through the membrane of the giant axon of *Loligo*. J Physiol (Lond) 117:449–472.

Hodgkin AL, Huxley AF (1952b) A quantitative description of membrane current and its application to conduction and excitation in nerve. J Physiol (Lond) 117:500–544.

Johansen J, Kleinhaus AL (1986) Transient and delayed potassium currents in the Retzius cell of the leech *macrobdella decora*. J Neurophysiol 56:812–822.

Jones SW, Adams PR (1987) The M-current and other potassium currents of vertebrate neurons. In: Neuromodulation—the biochemical control of neuronal excitability (Kaczmarek LK, Levitan IB, eds), pp 159–186. New York: Oxford UP.

Junge D (1985) Calcium dependence of A-currents in perfused *Aplysia* neurons. Brain Res 346:294–300.

Kuhlman JR, Li C, Calabrese RL (1985a) FMRF-amide-like substances in the leech. I. Immunocytochemical localization. J Neurosci 5:2301–2309.

Kuhlman JR, Li C, Calabrese RL (1985b) FMRF-amide-like substances in the leech. II. Bioactivity on the heartbeat system. J Neurosci 5:2310–2317.

Kupfermann I (1979) Modulatory actions of neurotransmitters. Annu Rev Neurosci 2:447–465.

MacDermott AB, Weight FF (1982) Action potential repolarization may involve a transient, Ca^{2+}-sensitive outward current in a vertebrate neurone. Nature 300:185–188.

Madison DV, Lancaster B, Adams PR (1987) Voltage clamp analysis of cholinergic action in the hippocampus. J Neurosci 7:733–741.

Marder E, Hooper S (1985) Neurotransmitter modulation of the stomatogastric ganglion of decapod crustaceans. In: Model neural networks & behavior (Selverston AI, ed), pp 316–337. New York: Plenum.

Marder E, Meyrand P (1989) Chemical modulation of an oscillatory neural circuit. In: Neuronal & cellular oscillators (Jacklet JW, ed). New York: Dekker.

Marder E, Nusbaum MP (1989) Peptidergic modulation of the motor pattern generators in the stomatogastric ganglion. In: Perspectives in neural systems & behavior (Carew TJ, Kelley DB, eds), pp 73–92. New York: Liss.

Meech RW, Standen NB (1975) Potassium activation in *Helix aspersa* neurones under voltage clamp: a component mediated by calcium influx. J Physiol (Lond) 249:211–239.

Nicholls JG, Kuffler SW (1965) Na and K content of glial cells and neurons determined by flame photometry in the central nervous system of the leech. J Neurophysiol 29:788–806.

Nicholls JG, Wallace BG (1978) Modulation of transmission at an inhibitory synapse in the central nervous system of the leech. J Physiol (Lond) 281:157–170.

Rudy B (1988) Diversity and ubiquity of K channels. Neuroscience 25:729–749.

Schwarz JR, Vogel W (1971) Potassium inactivation in single myelinated nerve fibers of *Xenopus laevis*. Pfluegers Arch 330:61–73.

Siegelbaum SA (1987) The S-current—a background potassium current. In: Neuromodulation—the biochemical control of neuronal excitability (Kaczmarek LK, Levitan IB, eds), pp 187–205. New York: Oxford UP.

Siegelbaum SA, Tsien RW (1980) Calcium activated transient outward current in calf cardiac Purkinje fibres. J Physiol (Lond) 299:485–506.

Stewart RR, Nicholls JG, Adams WB (1989) Na^+, K^+, and Ca^{2+} currents in identified leech neurones in culture. J Exp Biol 141:1–20.

Strong JA, Kaczmarek LK (1987) Potassium currents that regulate action potentials and repetitive firing. In: Neuromodulation—the biochemical control of neuronal excitability (Kaczmarek LK, Levitan IB, eds). New York: Oxford UP.

Takenaka T, Horie H, Hori H, Kawakami K (1988) Effects of arachidonic acid and other long-chain fatty acids on the membrane currents in the squid giant axon. J Membr Biol 106:141–147.

Thompson SH (1977) Three pharmacologically distinct potassium channels in molluscan neurones. J Physiol (Lond) 265:465–488.

Thompson WJ, Stent GS (1976) Neuronal control of heartbeat in the medicinal leech. III. Synaptic relations of the heart interneurons. J Comp Physiol 111:281–307.

Tolbert LP, Calabrese RL (1985) Anatomical analysis of contacts between identified neurons that control heartbeat in the leech, *Hirudo medicinalis*. Cell Tissue Res 242:257–267.

Tsien RW, Giles WR, Greengard P (1972) Cyclic AMP mediates the action of norepinephrine on the action potential plateau of cardiac Purkinje fibres. Nature 240:181–183.

Weeks JC, Kristan WB (1978) Initiation, maintenance and modulation of swimming in the medicinal leech by activity of a single neurone. J Exp Biol 77:71–88.

Yamada WM, Koch C, Adams PR (1989) Multiple channels and calcium dynamics. In: Methods in neuronal modeling (Koch C, Segev I, eds), pp 97–134. Cambridge: MIT Press.